www.ietdl.org

Published in IET Power Electronics
Received on 23rd September 2011
Revised on 21st August 2012
doi: 10.1049/iet-pel.2011.0361

ISSN 1755-4535

Transient and steady-state analysis of three-phase PWM buck rectifier

N. Krihely M.A. Slonim S. Ben-Yaakov

Power Electronics Laboratory, Department of Electrical and Computer Engineering, Ben-Gurion University of the Negev, P.O.Box 653, Beer-Sheva 84105, Israel
E-mail: krikali@ee.bgu.ac.il

Abstract: This study presents a qualitative and quantitative analysis of the output current response of a three-phase buck rectifier. The DC-side of the three-phase pulse-width modulation (PWM) buck rectifier is loaded by a typical series equivalent circuit comprising a resistor, an inductor and a constant voltage. An analytical solution of transient and steady-state processes is obtained using the difference equation method in the continuous conduction mode. The proposed analytical solution exhibits two repetition intervals, which accurately predict the ripple components of the output current. Hence, the solution of the process envelopes is obtained. The derivation of the plant transfer function from the analytical solution of the output current is also presented. System simulations and experimental studies are carried out to validate the analytical approach with various output loads.

1 Introduction

Frequently, in many power conversion applications, it is required to power a typical load with an equivalent circuit composed of a series resistor R_o, an inductor L_o and a constant voltage V_o. For example, small-scale low-power wind turbines are commonly used to charge battery systems of 12 V or higher [1]. Specifically, in this kind of application the series inductance and the resistance approach negligible values, whereas the constant voltage V_o that reflects the battery, dominates. In a battery-charging system, the type of rectifier required for the power conversion process is determined by the nature of the source and by the battery bank voltage. In other cases, such a typical load can describe the electrical side of a DC motor. Here, the resistor, the inductance and the constant voltage of the load represent the armature resistance, the inductance and the back electromotive force (EMF) of the motor, respectively. In some situations, the constant voltage, V_o, can be discarded completely, as often occurs, for example, when the load is a stove for supplying heat. One possible solution for the above applications is the three-phase PWM rectifier shown in Fig. 1 [2, 3]. The rectifier employs three switches, Q_R, Q_S and Q_T, and 12 diodes. An additional freewheeling diode, D_{FW}, ensures continuity of the DC-side output current, i_o. This circuit (Fig. 1) can roughly be classified as a single-stage processing system with high-quality input currents. In practice, this rectifier can also be a solution for medium power and high input voltage applications such as telecom power supplies [2] and uninterruptible power supply (UPS) systems. For many years, theoretical analyses of rectifiers were the primary focus of research in conventional line-commutated rectifiers [4, 5]. The main advantage of the PWM rectifier application lies in the possibility to accurately control the harmonic content of the output current, i_o, as well as to power a variety of loads more effectively. However, the main drawback of the rectifier lies in the number of diodes, which undermine its advantages as a single-stage power processing system. This could be a concern, especially when high step-down ratios are applied, such as in low input voltage applications. In order to optimise the output power delivered to the load, the relationship between the changes of output current, i_o, and the modulation index, M, needs to be known. The role of the modulation index, M, of three-phase PWM rectifiers is equivalent to the role of the duty cycle, D, used in DC–DC converters. It is clear that an analytical representation of the output current, i_o, process in terms of circuit parameters will yield the required dependence on the modulation index, M. Furthermore, this expression constitutes the basis for other properties that can be derived, such as the power stage transfer function, the output current step response and transient and steady-state behaviours. However, the PWM rectifier is a non-linear circuit and obtaining an analytical, closed form solution for such circuits (Fig. 1) has not been presented in the scientific literature. A mathematical analysis of a four-switch three-phase PWM rectifier is presented in [6]. This analysis investigated the steady-state behaviour of the line currents based on the mixed $p-z$ approach. Three-phase rectifiers are generally modelled by state-space averaging of an equivalent DC–DC converter [7]. Previous studies have shown that a closed-form analytical solution of DC–DC boost and buck converters can be found using the difference equation method [8].

In this paper, an analytical expression of the output current, i_o, process in terms of circuit parameters will be derived, based on the difference equation method [9]. This approach enables obtaining a closed form solution of the output

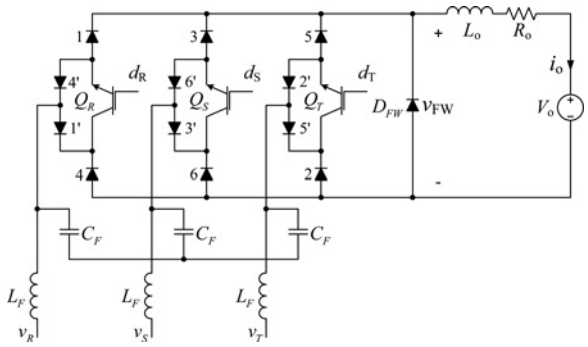

Fig. 1 *General topology of a three-phase buck rectifier*

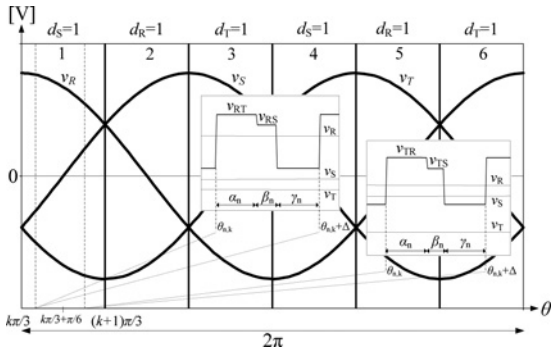

Fig. 2 *Input phase voltages, v_R, v_S, v_T, divided into six sectors of $\pi/3$ and voltage changes during switching interval Δ*

The notation $d_i = 1$ (i = R, S, T) represents a logical high state applied to the gate

current under both transient and steady-state operation. In addition, small-signal properties of the rectifier are directly obtained from the analytical expression of the output current response. To verify the validity of the proposed approach, the theoretical results were compared to simulation data and experimental measurements.

2 Qualitative analysis of the rectifier operation

The general circuit diagram of the three-phase rectifier is depicted in Fig. 1. The input filter L_F, C_F between the AC source and the rectifier input is necessary for attenuating high switching frequency harmonics. For the following analysis the input phase voltages are defined herein as

$$\begin{aligned} v_R &= V_m \cos\left(\theta - k\frac{\pi}{3}\right) \\ v_S &= V_m \cos\left(\theta - k\frac{\pi}{3} - \frac{2\pi}{3}\right) \\ v_T &= V_m \cos\left(\theta - k\frac{\pi}{3} + \frac{2\pi}{3}\right) \end{aligned} \tag{1}$$

where, $\theta = \omega_L t$ is the instantaneous phase angle, ω_L is the angular frequency of the source, V_m is the input phase voltage amplitude and the index $k = \{0, 1, 2,\ldots\}$ denotes a sector with length of $\pi/3$. Let us represent the PWM switching period, T_s, by an equivalent switching interval, $\Delta = 2\pi T_s/T_L$, where $T_L = 2\pi/\omega_L$ is the period of the source. The following calculations will be based on the analysis of the process during Δ intervals. Therefore it is convenient to express instantaneous phase as follows

$$\theta_{n,k} = k\frac{\pi}{3} + n\Delta \tag{2}$$

where $n = \{0, 1, \ldots, N-1\}$ denotes the subinterval index resulting from the PWM switching process, such that $N = \pi/(3\Delta)$. Fig. 2 depicts the phase voltages divided into six sectors of $\pi/3$. The figure also highlights the time behaviour of the input phases, v_R, v_S, v_T at $\theta_{n,k}$ throughout one switching period, Δ, resulting from the PWM switching. Several possibilities exist for arranging the switching sequence of the rectifier within one switching period. However, one sequence arrangement may be advantageous over the others, depending on the required performances. Fig. 3 illustrates the switching sequence used in this work, valid for $k\pi/3 \le \theta \le (k+1)\pi/3$. This modulation sequence is chosen mainly for computational convenience of the mathematical concept. The switching strategy of the PWM technique is detailed below. The signals d_R, d_S and d_T (Fig. 3) are applied to the gates of the switches Q_R, Q_S and Q_T, respectively. To better clarify the operation principle of the rectifier and to build the required foundation for the upcoming analysis, the following fundamental assumptions are made:

(1) To simplify the involved mathematics, the analysis refers to the particular case in which $L_F = C_F = 0$. This is equivalent to the case where the voltage drops of the generator stator inductances are small enough to be neglected. Hence, the terminal voltages can be considered to be equal to the back EMFs of the generator. For example, micro-scale wind generators [10] and true three-phase AC sources comply with this condition.
(2) All switches and diodes are ideal.
(3) Operation mode of the DC side inductor L_o is continuous conduction mode.

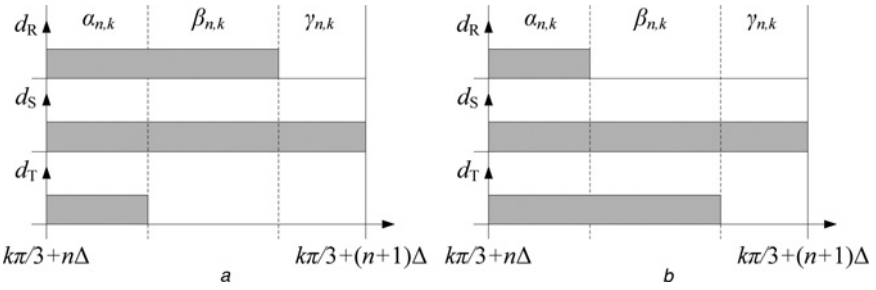

Fig. 3 *Switching pattern and conduction states during one switching period, Δ, within*

a $k\pi/3 \le \theta \le k\pi/3 + \pi/6$
b $k\pi/3 + \pi/6 \le \theta \le (k+1)\pi/3$

(4) In order to obtain a resistive behaviour between the fundamental input current and the phase voltage, the firing angles of the switches are set to zero.
(5) The switches of the rectifier are operated with a high frequency PWM template.
(6) Since the switching frequency f_s is much higher than the frequency of the source f_L namely, $f_s \gg f_L$, during a single switching interval, Δ, the voltage is regarded constant at any phase. This statement is also illustrated in Fig. 2 using one switching interval of the signals v_R, v_S and v_T.

Thus, proper operation of the rectifier with PWM control will be achieved.

In order to derive the relative 'on' times of the three switches, the firing assumptions of the PWM strategy are defined as follows:
(7) The 'on' time interval of the switches will depend on the respective phase voltage value sampled at the beginning of the switching period, Δ (Fig. 3).
(8) In order to adjust the fundamental component of the input currents to be proportional to the corresponding input voltages, the conduction time of the three switches are

$$\psi_i = M\frac{|v_i(\theta_{n,k})|}{V_m} \tag{3}$$

where $i = \{R, S, T\}$ and M is the modulation index such that $0 \le M \le 1$. The instantaneous phase, $\theta_{n,k}$, is defined in (2) and depicted in Fig. 2.
(9) The rectifier switch corresponding to the smallest magnitude phase voltage is held 'on' throughout an interval of $\pi/3$ (Figs. 2 and 3).
(10) During any switching interval, Δ, the duty cycle of the two remaining switches is set in proportion to the corresponding instantaneous phase voltage samples as defined in (3).
(11) At any time, only two of the three legs of the bridges are conducting.
(12) Conduction time of any transistor pair depends on the corresponding smallest absolute voltage between the two.

We note that the index k reflects the repetition period of the rectifier with an interval of $\pi/3$ (Fig. 2). It will be shown that by analysing the behaviour of the rectifier during a $\pi/3$ interval, a difference equation that describes the transient and the steady-state processes will be obtained. It has been shown that application of difference equations analysis to PWM converters requires determination of the repetition period [8, 9], which is the time interval over which all possible changes in the converter's topologies occur. As already stated, the repetition interval of the converter bridge is $\pi/3$. However, application of PWM switching reduces the repetition interval up to Δ, which is the interval between two sequenced ignitions of switches pair.

Owing to the symmetry of the input phases the following analysis of the circuit operation will be focused over an interval of $k\pi/3 \le \theta \le (k+1)\pi/3$. However, for the remaining sectors the analysis may be conducted in an analogue manner. Fig. 4 summarises the equivalent topologies associated with each conduction state during a switching interval, Δ, in the considered sector $k\pi/3 \le \theta \le (k+1)\pi/3$.

Each switch ignition leads to two diodes conducting (Fig. 1). Thus, assuming that switches Q_R and Q_S are ignited and $v_R > v_S$, then diodes 1, 1′ and 6, 6′ will conduct, or alternatively, diodes 4, 4′ and 3, 3′ will conduct when $v_S > v_R$. In this way, the rectifier operates similarly to the operation of a regular three-phase bridge.

As is evident in Fig. 3, every switching interval, Δ, comprises a sequence of three conduction states; two active states with relative 'on' times $\alpha_{n,k}$, $\beta_{n,k}$ and a freewheeling state with the relative time $\gamma_{n,k}$. During the two active states the output current, i_o, is switched between two transistor pairs, whereas in the third state the output current flows through the freewheeling diode D_{FW}. For each conduction state a line-to-line voltage is propagated to the DC side of the rectifier as a voltage, v_{FW}.

To gain a better insight into circuit operation, let us first analyse the resulting process during the sub-sector $k\pi/3 \le \theta \le k\pi/3 + \pi/6$ (Fig. 3*a*) with reference to the diagram depicted in Fig. 4. During the first active state, $\alpha_{n,k}$, the largest line-to-line voltage is v_{RT} (Fig. 2); thus, the Q_R–Q_T pair will conduct the output current, i_o (Fig. 4*a*). According to assumptions 7–12, the relative 'on' time, $\alpha_{n,k}$, and the respective v_{FW} voltage can be expressed as

$$\begin{aligned}\alpha_{n,k} &= \psi_T\Delta = -M\Delta\cos\left(\theta_{n,k} - k\frac{\pi}{3} + \frac{2\pi}{3}\right)\\ v_{FW} &= v_R - v_T = V_{LL}\cos\left(\theta_{n,k} - k\frac{\pi}{3} - \frac{\pi}{6}\right)\end{aligned} \tag{4}$$

where $V_{LL} = \sqrt{3}V_m$. During the second active state, $\beta_{n,k}$, the second largest line-to-line voltage is v_{RS} (Fig. 2); thus, the Q_R–Q_S pair will conduct i_o (Fig. 4*b*). In this condition the relative 'on' time, $\beta_{n,k}$, and the respective v_{FW} voltage are expressed as

$$\begin{aligned}\beta_{n,k} &= (\psi_R - \psi_T)\Delta = -M\Delta\cos\left(\theta_{n,k} - k\frac{\pi}{3} - \frac{2\pi}{3}\right)\\ v_{FW} &= v_R - v_S = V_{LL}\cos\left(\theta_{n,k} - k\frac{\pi}{3} + \frac{\pi}{6}\right)\end{aligned} \tag{5}$$

In the freewheeling state, $\gamma_{n,k}$, only Q_S is in the 'on' state since it corresponds to the smallest absolute phase voltage, v_S, throughout sector 1 (Fig. 2). Note that the freewheeling diode, D_{FW}, will always lead the conduction of the output current during state $\gamma_{n,k}$ according to the topology shown in Fig. 4*c*. The reason for this is because the output current conduction causes a higher voltage drop in one bridge leg (total forward voltage drop of one switch and two rectifier diodes) than that of a single diode. Hence, in this case the relative 'on' time, $\gamma_{n,k}$, and the respective v_{FW} voltage are expressed by

$$\gamma_{n,k} = \Delta - \alpha_{n,k} - \beta_{n,k},\ v_{FW} = 0 \tag{6}$$

Correspondingly, for the second sub-sector $k\pi/3 + \pi/6 \le \theta \le (k+1)\pi/3$ (Figs. 3*b* and 4*d*–*f*) it can be shown that (4)–(6) are translated to

$$\begin{aligned}\alpha_{n,k} &= \psi_R\Delta = M\Delta\cos\left(\theta_{n,k} - k\frac{\pi}{3}\right)\\ v_{FW} &= v_T - v_R = V_{LL}\cos\left(\theta_{n,k} - k\frac{\pi}{3} - \frac{\pi}{6}\right)\end{aligned} \tag{7}$$

$$\begin{aligned}\beta_{n,k} &= (\psi_T - \psi_R)\Delta = M\Delta\cos\left(\theta_{n,k} - k\frac{\pi}{3} - \frac{2\pi}{3}\right)\\ v_{FW} &= v_T - v_S = V_{LL}\cos\left(\theta_{n,k} - k\frac{\pi}{3} - \frac{\pi}{2}\right)\end{aligned} \tag{8}$$

$$\gamma_{n,k} = \Delta - \alpha_{n,k} - \beta_{n,k},\ v_{FW} = 0 \tag{9}$$

doi: 10.1049/iet-pel.2011.0361

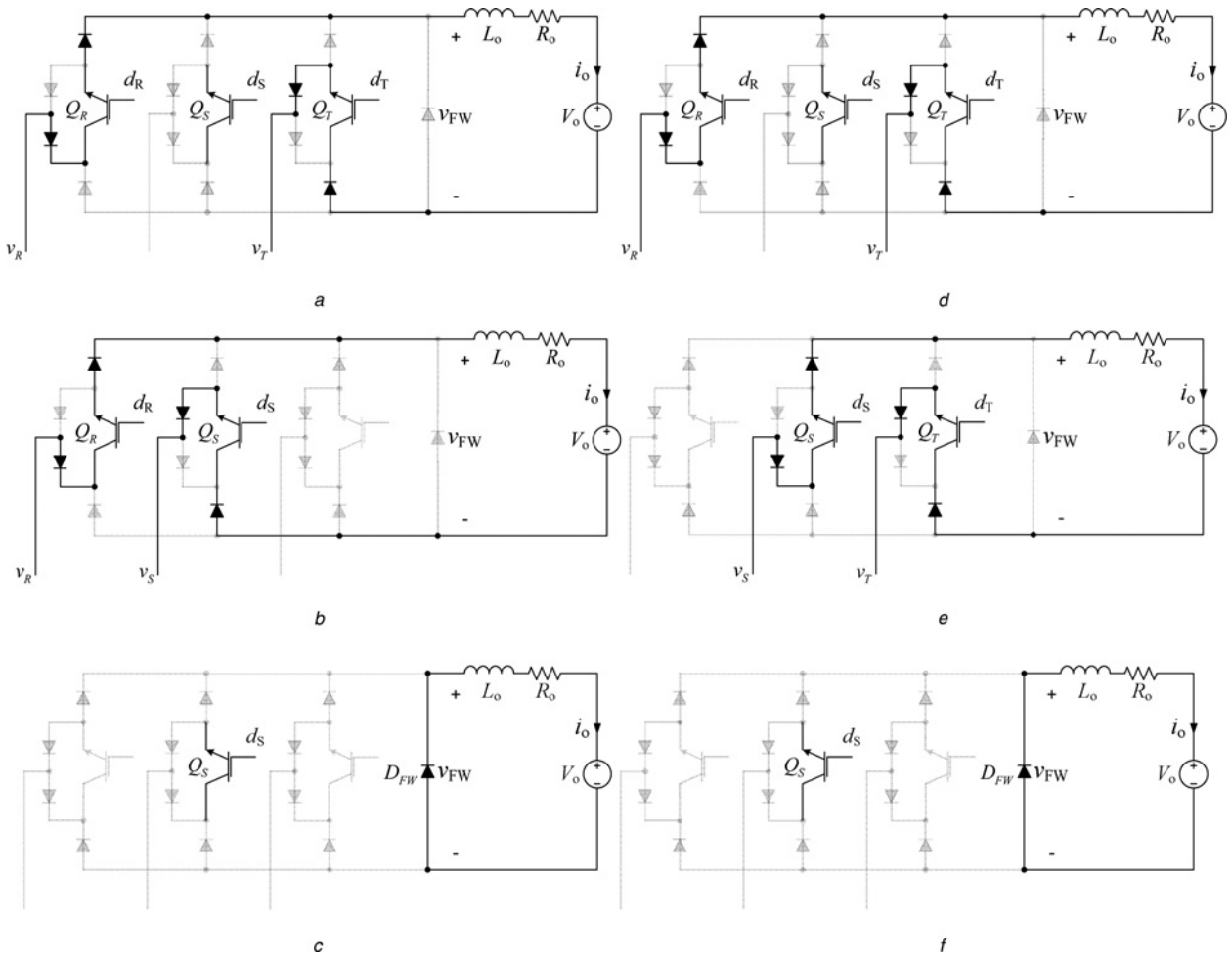

Fig. 4 *Operation topologies of one switching period Δ*

Conduction states within $k\pi/3 \le \theta \le k\pi/3 + \pi/6$
a State $\alpha_{n,k}$
b State $\beta_{n,k}$
c State $\gamma_{n,k}$
Conduction states within $k\pi/3 + \pi/6 \le \theta \le (k+1)\pi/3$
d State $\alpha_{n,k}$
e State $\beta_{n,k}$
f State $\gamma_{n,k}$
See also Fig. 3 for notations

We can see that $\alpha_{n,k}$, $\beta_{n,k}$ and the respective line-to-line voltage during the second conduction state are changing every $\pi/6$. In order to express the last three equations for each possible sector with the correct relationship to the instantaneous phase angle, $\theta_{n,k}$, an auxiliary parameter ε is introduced

$$\varepsilon = \begin{cases} 0, & k\dfrac{\pi}{3} \le \theta_{n,k} \le k\dfrac{\pi}{3} + \dfrac{\pi}{6} \\ 1, & k\dfrac{\pi}{3} + \dfrac{\pi}{6} \le \theta_{n,k} \le (k+1)\dfrac{\pi}{3} \end{cases} \tag{10}$$

Applying (10), the general form of (4)–(9) for any possible sector, k and $\theta_{n,k}$ can be expressed as

$$\begin{aligned} \alpha_{n,k} &= (-1)^{\varepsilon+1} M\Delta \cos\left[\theta_{n,k} - k\frac{\pi}{3} + \frac{\pi}{3} + \frac{\pi}{3}(-1)^{\varepsilon}\right] \\ v_{FW} &= V_{LL} \cos\left(\theta_{n,k} - k\frac{\pi}{3} - \frac{\pi}{6}\right) \end{aligned} \tag{11}$$

$$\begin{aligned} \beta_{n,k} &= (-1)^{\varepsilon+1} M\Delta \cos\left(\theta_{n,k} - k\frac{\pi}{3} - \frac{2\pi}{3}\right) \\ v_{FW} &= V_{LL} \cos\left[\theta_{n,k} - k\frac{\pi}{3} - \frac{\pi}{6} + \frac{\pi}{3}(-1)^{\varepsilon}\right] \end{aligned} \tag{12}$$

$$\gamma_{n,k} = \Delta - \alpha_{n,k} - \beta_{n,k},\ v_{FW} = 0 \tag{13}$$

Applying (2), (11)–(13) further reduce to

$$\begin{aligned} \alpha_n &= (-1)^{\varepsilon+1} M\Delta \cos\left[n\Delta + \frac{\pi}{3} + \frac{\pi}{3}(-1)^{\varepsilon}\right] \\ v_{FW} &= V_{LL} \cos\left(n\Delta - \frac{\pi}{6}\right) \end{aligned} \tag{14}$$

$$\begin{aligned} \beta_n &= (-1)^{\varepsilon+1} M\Delta \cos\left(n\Delta - \frac{2\pi}{3}\right) \\ v_{FW} &= V_{LL} \cos\left[n\Delta - \frac{\pi}{6} + \frac{\pi}{3}(-1)^{\varepsilon}\right] \end{aligned} \tag{15}$$

$$\gamma_n = \Delta - \alpha_n - \beta_n,\ v_{FW} = 0 \tag{16}$$

where α_n, β_n, γ_n now depend only on the index n.

It is clear that the current in the DC inductor is determined by the line-to-line voltage propagated to the DC side, v_{FW}, and by the constant voltage, V_o. As a result, the DC inductor current experiences two ripple components. One is due to the high frequency PWM switching process, which is related to Δ, and the second one is originates from the rectification process of the diode bridge and has a periodicity of $\pi/3$. To find an analytical solution to the problem, one should analyse the output current process over interval $k\pi/3 + n\Delta \le \theta \le k\pi/3 + (n+1)\Delta$ for any value of k and n.

3 Analytical approach

Let us assume that analysis of the process starts with ignition of the switches Q_R–Q_T (Fig. 4*a*) at the instant $\theta = k\pi/3 + n\Delta$ (which is equal to $\theta_{n,k}$ as shown in Fig. 2). The computation of the output current process over the switching interval $k\pi/3 + n\Delta \le \theta \le k\pi/3 + (n+1)\Delta$ is governed by first order differential equations. The differential equation which reflect the behaviour of the first RT topology is given by

$$\omega_L L_o \frac{di_o}{d\theta} + R_o i_o + V_o = v_{RT} \tag{17}$$

applying (14)

$$\omega_L L_o \frac{di_o}{d\theta} + R_o i_o = V_{LL}\cos\left(n\Delta - \frac{\pi}{6}\right) - V_o \tag{18}$$

Using the Laplace transform technique, the solution of (18) is found to be (see (19))

$$i_o(\theta) = i_o[n,k]e^{-(\theta - k(\pi/3) - n\Delta)/\omega_L\tau} + \frac{V_{LL}\cos(n\Delta - (\pi/6)) - V_o}{R_o}\left[1 - e^{-(\theta - k(\pi/3) - n\Delta)/\omega_L\tau}\right] \tag{19}$$

where $i_o[n, k] = i_o(\theta = k\pi/3 + n\Delta)$ is the initial condition of the current at $\theta = k\pi/3 + n\Delta$ and $\tau = L_o/R_o$ is time constant.

The RT topology is valid up to $\theta = k\pi/3 + n\Delta + \alpha_n$ (Fig. 3*a*) when the switch Q_T ceases to conduct and the switch Q_S starts to conduct (Fig. 4*b*). At that instant the process enters the second state with an interval of $k\pi/3 + n\Delta + \alpha_n \le \theta \le k\pi/3 + n\Delta + \alpha_n + \beta_n$. The differential equation of the circuit is therefore

$$\omega_L L_o \frac{di_o}{d\theta} + R_o i_o + V_o = v_{RS} \tag{20}$$

where the conduction time β_n and output voltage v_{RS} expressions are as given in (15). Substituting the proper v_{RS} expression into (20) we obtain

$$\omega_L L_o \frac{di_o}{d\theta} + R_o i_o = V_{LL}\cos\left[n\Delta - \frac{\pi}{6} + \frac{\pi}{3}(-1)^{\varepsilon}\right] - V_o \tag{21}$$

The output current is computed as

$$i_o(\theta) = i_o(\alpha_n)\,e^{-(\theta - k(\pi/3) - n\Delta - \alpha_n)/\omega_L\tau} + \frac{V_{LL}\cos[n\Delta - (\pi/6) + (\pi/3)(-1)^{\varepsilon}] - V_o}{R_o} \times \left[1 - e^{-\frac{(\theta - k(\pi/3) - n\Delta - \alpha_n)}{\omega_L\tau}}\right] \tag{22}$$

where $i_o(\alpha_n) = i_o(\theta = k\pi/3 + n\Delta + \alpha_n)$.

The switches Q_R–Q_S cease to conduct at the instant $\theta = k\pi/3 + n\Delta + \alpha_n + \beta_n$, when the freewheeling diode D_{FW} starts to conduct (Fig. 4*c*). The freewheeling diode conducts during an interval γ_n up to the instant $\theta = k\pi/3 + (n+1)\Delta$ (Fig. 3*a*). Repeating the above techniques we can find the solution of the third freewheeling state during $k\pi/3 + n\Delta + \alpha_n + \beta_n \le \theta \le k\pi/3 + (n+1)\Delta$. The differential equation of the third topology and the appropriate solution for it are given in (23) and (24), respectively.

$$\omega_L L_o \frac{di_o}{d\theta} + R_o i_o = -V_o \tag{23}$$

$$i_o(\theta) = i_o(\beta_n)e^{-(\theta - k(\pi/3) - n\Delta - \alpha_n - \beta_n)/\omega_L\tau} - \frac{V_o}{R_o}\left[1 - e^{-(\theta - k(\pi/3) - n\Delta - \alpha_n - \beta_n)/\omega_L\tau}\right] \tag{24}$$

where $i_o(\beta_n) = i_o(\theta = k\pi/3 + n\Delta + \alpha_n + \beta_n)$.

To determine the connection between the three states of the circuit for any repetition period during $k\pi/3 + n\Delta \le \theta \le k\pi/3 + (n+1)\Delta$ we need to connect the boundaries of above three expressions (19), (22) and (24). This operation yields to an equivalent difference equation with the general form (see Appendix for details)

$$i_o[n+1, k] - i_o[n, k]\xi = F_n(M) \tag{25}$$

where $F_n(M)$ is a function of the modulation index M (see (26))

and

$$\xi = e^{-\Delta/\omega_L\tau} \tag{27}$$

To obtain a closed form solution of the difference equation, the number of independent variables must be reduced. The procedure for removing dependency on the discrete variable n is carried out by summing a set of local difference

$$F_n(M) = -\frac{V_o}{R_o} - \frac{V_{LL}\cos(n\Delta - (\pi/6)) - V_o}{R_o}\,e^{-\Delta/\omega_L\tau} + \frac{V_{LL}\cos[n\Delta - (\pi/6) + (\pi/3)(-1)^{\varepsilon}]}{R_o}\,e^{-(\Delta - \alpha_n - \beta_n)/\omega_L\tau} - \left(\frac{V_{LL}\cos[n\Delta - (\pi/6) + (\pi/3)(-1)^{\varepsilon}]}{R_o} - \frac{V_{LL}\cos(n\Delta - (\pi/6))}{R_o}\right)e^{-(\Delta - \alpha_n)/\omega_L\tau} \tag{26}$$

doi: 10.1049/iet-pel.2011.0361

equations over an arbitrary sector $\pi/3$ as follows

$$\begin{aligned} & i_o[1, k] - i_o[0, k]\xi = F_0(M) \\ & \vdots \\ & i_o[N, k] - i_o[N-1, k]\xi = F_{N-1}(M) \end{aligned} \tag{28}$$

This operation links the boundaries of the kth repetition interval such that the difference equation for the $\pi/3$ interval is obtained

$$i_o[k+1] - i_o[k]\lambda = F_\Sigma(M) \tag{29}$$

where

$$\lambda = \prod_{n=0}^{N-1} \xi = \xi^N, \; F_\Sigma(M) = \sum_{n=0}^{N-1} \{F_n(M) \cdot \xi^{N-1-n}\} \tag{30}$$

A closed-form solution of the difference equation is given by

$$i_o[k] = F_\Sigma(M)\frac{1-\lambda^k}{1-\lambda} + i_o[0]\lambda^k \tag{31}$$

where $i_o[0]$ is the initial condition at $k = 0$. Since λ is less than one, the transient component λ^k will eventually die out. Note that (31) enables us to find $i_o[k]$ under steady-state conditions by substituting $k = \infty$. Thus, it follows that

$$i_o[k]_{ST} = \frac{F_\Sigma(M)}{1-\lambda} \tag{32}$$

where $i_o[k]_{ST}$ is the steady-state value of $i_o[k]$ and the subscript ST denotes steady state.

4 Small signal analysis

In practical applications, the output current i_o needs to be controlled in order to follow a current reference I_{ref}. For this, the dynamic behaviour of the rectifier at different operating points should be known. It can be shown that the control to output discrete transfer function $G(z)$ can be derived from the general difference (25). Let us introduce some AC variation into the converter signals given by

$$\begin{aligned} i_o[n, k] &= I + \hat{i}_o[n, k] \\ m[n, k] &= M + \hat{m}[n, k] \end{aligned} \tag{33}$$

where I is the DC current component during interval Δ and M is the modulation index. The symbol $(\hat{\cdot})$ represents the small signal quantity. Equation (25) may also expressed as a function of $i_o[n, k]$ and $F_n(M)$

$$i_o[n+1, k] = i_o[n, k]\xi + F_n(M) \tag{34}$$

The linearised small signal difference equation of (34) centred about the operating point may be expressed as

$$\hat{i}_o[n+1, k] = a_o\hat{i}_o[n, k] + b_o\hat{m}[n, k] \tag{35}$$

The coefficients a_o and b_o are calculated as (see (36)) where (see (37))

The coefficient b_o is obtained by averaging the partial derivative (37) over a $\pi/3$ interval. Applying the Z-transform to the difference (35), the transfer function of the plant is found to be

$$G(z) = \frac{\hat{i}_o(z)}{\hat{m}(z)} = \frac{b_o}{z - a_o} \tag{38}$$

The analytical expression of $G(z)$ is very useful for calculating the discrete current step response. If we introduce a small step, δ_m, in the modulation index, M, such that $m[n, k] = M + \delta_m u[n, k]$ (where $u[n, k]$ is the discrete step function), then by substituting the above small signal parameters a_o, b_o it follows that

$$\begin{aligned} \hat{i}_o[n, k] &= Z^{-1}\{G(z) \cdot \hat{m}(z)\} = Z^{-1}\left\{\frac{b_o}{z-a_o}\delta_m\frac{z}{z-1}\right\} \\ &= \delta_m b_o \frac{1-a_o^n}{1-a_o} \end{aligned} \tag{39}$$

where $Z^{-1}\{\cdot\}$ represents the inverse Z-transform operation. Substituting $a_o = \xi$, it is clear that

$$\hat{i}_o[n, k]_{ST} = \frac{\delta_m b_o}{1-\xi} \tag{40}$$

where $\hat{i}_o[n, k]_{ST}$ is the steady-state value of (39).

5 Analytical and simulation results

To confirm the effectiveness of the mathematical approach, the analytical results are visualised using Mathcad and compared to the results obtained by applying the rectifier circuit to a PSIM simulator. Fig. 5 shows the schematic diagram of the simulation setup for validating the analytical

$$\begin{aligned} a_o &= \left.\frac{\partial\{i_o[n, k]\xi + F_n(M)\}}{\partial i_o[n, k]}\right|_Q = \xi \\ b_o &= \left.\frac{1}{N}\sum_{n=0}^{N-1}\frac{\partial\{i_o[n, k]\xi + F_n(M)\}}{\partial M}\right|_Q = \left.\frac{1}{N}\sum_{n=0}^{N-1}\frac{\partial F_n(M)}{\partial M}\right|_Q \end{aligned} \tag{36}$$

$$\begin{aligned} \frac{\partial F_n(M)}{\partial M} &= \frac{V_{LL}\cos[n\Delta - (\pi/6) + (\pi/3)(-1)^\varepsilon]}{R_o}\frac{(\alpha_n/M) + (\beta_n/M)}{\omega_L\tau}e^{-(\Delta-\alpha_n-\beta_n)/\omega_L\tau} \\ &\quad - \left(\frac{V_{LL}\cos[n\Delta - (\pi/6) + (\pi/3)(-1)^\varepsilon]}{R_o} - \frac{V_{LL}\cos(n\Delta - (\pi/6))}{R_o}\right)\frac{\alpha_n/M}{\omega_L\tau}e^{-(\Delta-\alpha_n)/\omega_L\tau} \end{aligned} \tag{37}$$

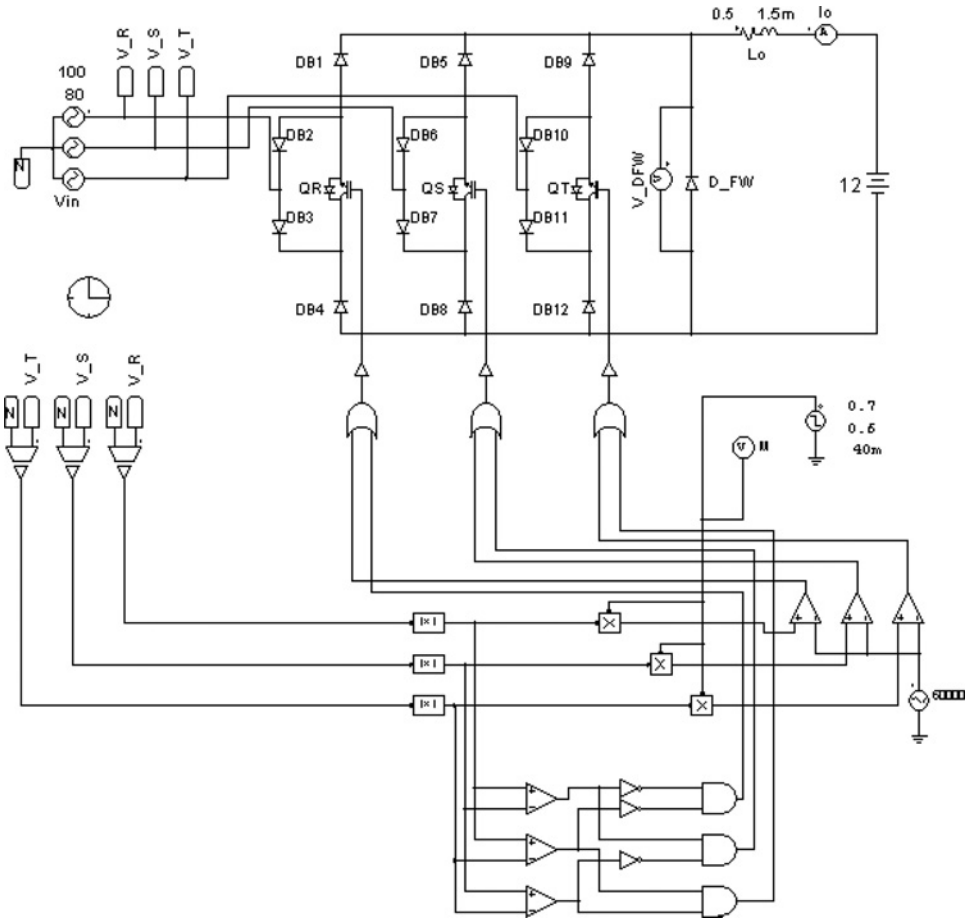

Fig. 5 *Simulation circuit of the rectifier and its control elements*

results. Fig. 6 depicts the Mathcad solution of the general difference equation $i_o[n, k]$ (25) and the PSIM simulation result with the following parameter values: $L_o = 100\ \mu H$, $R_o = 0.5\ \Omega$, $f_L = 100$ Hz, $f_s = 60$ kHz, $V_{LL} = 113$ V, $V_o = 12$ V and $M = 0.6$. By substituting these parameters, the PWM period, Δ, is found to be $\Delta = \pi/300$, and the conduction intervals, α_n, β_n, γ_n, are calculated, respectively, in accordance with (14)–(16) for a particular n. For example, if we consider the case $n = 0$, we obtain $\alpha_n = 0.3\Delta$, $\beta_n = 0.3\Delta$ and $\gamma_n = 0.4\Delta$. Similarly, for $n = 20$, we obtain $\alpha_n = 0.4\Delta$, $\beta_n = 0.185\Delta$ and $\gamma_n = 0.415\Delta$. As can be seen from Fig. 6, Mathcad's computed result accurately agrees with the process response during transient and steady-state operation. Accurate envelope tracking is evident from the theoretical response, whereas the existence of a sixth harmonic as a result of bridge operation is predicted as well. The comparison between the calculated $i_o[k]$ waveform (31) and the PSIM simulation is illustrated in Fig. 7 with the same parameters as before, except with a larger value of inductance $L_o = 2$ mH. As is evident from this comparison, there is excellent agreement between simulated and analytical results. It is worth mentioning that the time duration of the transient process (the time until steady state is reached) is

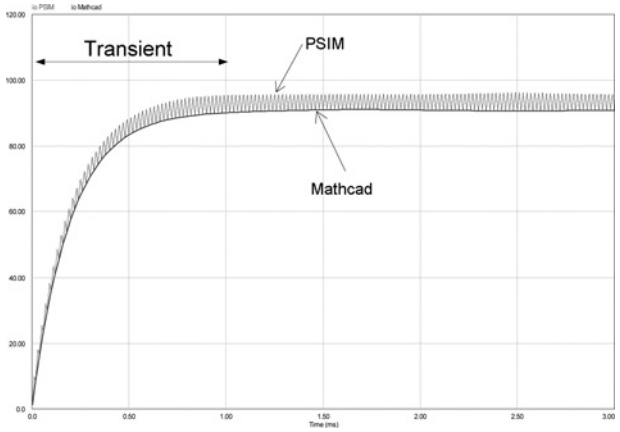

Fig. 6 *Computed and simulated output current response of $i_o[n, k]$ with the following parameter values: $L_o = 100\ \mu H$, $R_o = 0.5\ \Omega$, $f_L = 100$ Hz, $f_s = 60$ kHz, $V_{LL} = 113$ V, $V_o = 12$ V and $M = 0.6$*

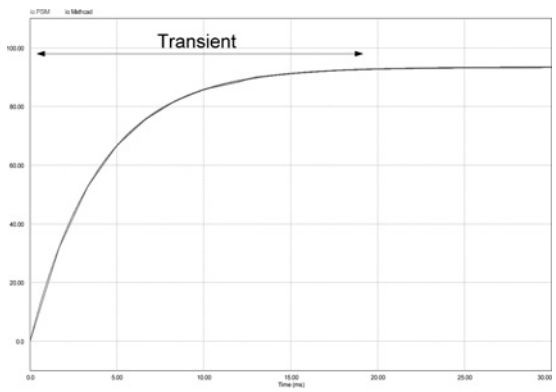

Fig. 7 *Computed and simulated output current response of $i_o[k]$ with the following parameter values: $L_o = 2$ mH, $R_o = 0.5\ \Omega$, $f_L = 100$ Hz, $f_s = 60$ kHz, $V_{LL} = 113$ V, $V_o = 12$ V and $M = 0.6$*

doi: 10.1049/iet-pel.2011.0361

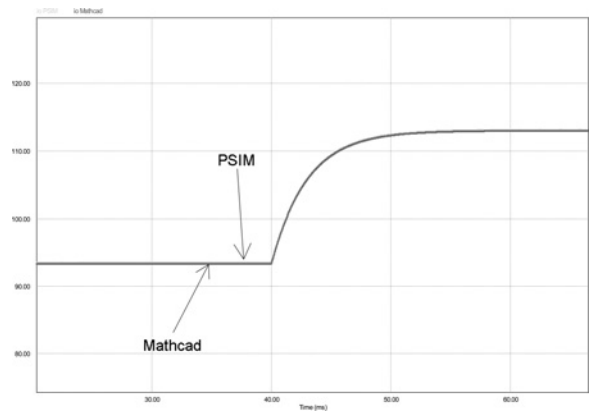

Fig. 8 *Computed and simulated output current response to a step $\delta_m = 0.1$ in modulation index with the same parameters as used in Fig. 7*

essentially controlled by the exponential terms ξ^n and λ^k of (25) and (31), respectively. Specifically, according to (27), these terms depend on the ratio $\Delta/\omega_L\tau$ (where $\tau = L_o/R_o$), which implies that for a larger L_o the transient process will be longer when the other parameters are kept constant. Substituting the corresponding parameter values, these terms are computed to be $\xi = 0.92$ and $\lambda = 0.659$. Therefore it can be concluded that the ξ^n and λ^k terms decay up to 0.01 when $n = 55$ and $k = 11$, implying that the transient has settled. The corresponding time durations until steady-state condition has been reached are 0.916 and 18 ms, respectively. These values perfectly match with the settling times when one extracts them from the simulated waveforms (Figs. 6 and 7).

The open-loop transient step response waveforms of $i_o[n, k]$ (39) and the PSIM simulation results are depicted in Fig. 8 for the same parameters used in Fig. 7, but with the introduction of a small step of $\delta_m = 0.1$ in the modulation index, M. As before, there is very good agreement between the analytical and simulation results. It can be seen that the settling time is about 12 ms. This time period also corresponds to the instance $n = 720$, for which the term ξ^n diminishes to 0.018.

Knowledge of the plant transfer function is mandatory for designing a suitable discrete current controller [11]. The plant discrete transfer function, $G(z)$ (38), and the transfer function, $G(f)$, as obtained from AC analysis in the PSIM simulator, are depicted in Fig. 9, evaluated with the following parameter values: $L_o = 100$ μH, $R_o = 0.05$ Ω, $f_L = 100$ Hz, $f_s = 60$ kHz, $V_{LL} = 85$ V, $V_o = 12$ V and $M = 0.5$. In this study, the PWM period and the sampling period are chosen to be equal. It is evident that the analytical transfer function, $G(z)$, can reflect faithfully the transfer function of the circuit. The usefulness of handling $G(z)$ mathematically stems from the ability to bypass the relatively long computation times generally associated with AC analysis of discrete-transition simulators [12].

6 Experimental study

The following experimental tests focus on validating the preceding theoretical approach for solving the steady state and transient response operation modes. To this end, a 50 Hz, three-phase, variable voltage source and an input filter with $L_F = 200$ μH, $C_F = 10$ μF were applied to the AC side of the rectifier. The control of the rectifier was realised by a fixed-point, 16-bit, 40 MIPS digital signal controller dsPIC33FJ16GS502. The digital signal controller generates the required firing signals d_R, d_S, d_T (see Fig. 3)

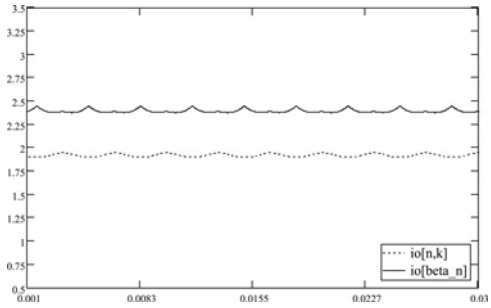

Fig. 10 *MathCAD's steady-state waveforms of the output current i_o with the following parameters: $L_o = 1.5$ mH, $R_o = 20.3$ Ω, $f_L = 50$ Hz, $f_s = 30$ kHz, $V_{LL} = 100$ V, $V_o = 12.4$ V and $M = 0.65$*

The waveforms $i_o[n, k]$ and $i_o(\beta_n)$ reflect the lower and upper envelop bounds of the actual response, respectively. Units: amperes against seconds

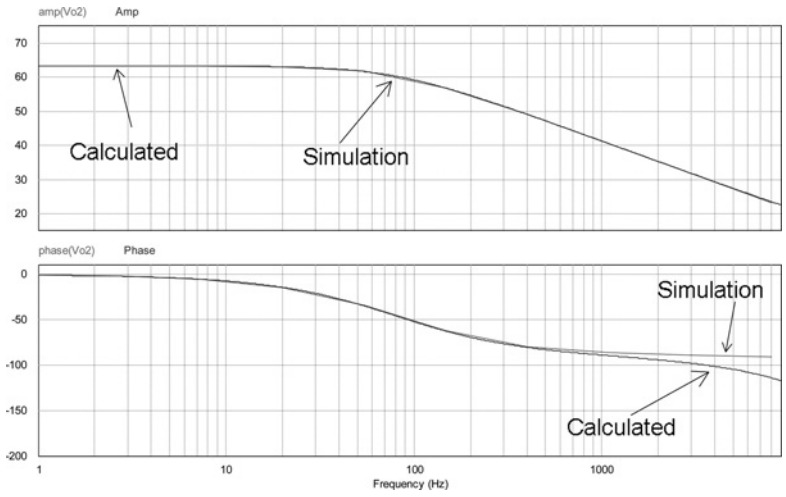

Fig. 9 *Calculated frequency response of the power stage plant G(z) and simulated frequency response G(f) obtained from AC analysis in PSIM with the following parameter values*

$L_o = 100$ μH, $R_o = 0.05$ Ω, $f_L = 100$ Hz, $f_s = 60$ kHz, $V_{LL} = 85$ V, $V_o = 12$ V and $M = 0.5$. Units: amplitude (upper traces) in dB and phase (lower traces) in degrees

for the PWM rectifier. Neglecting the voltage drops across the filter inductors (L_F), the voltages across the filter capacitors (C_F) are sensed by differential amplifiers and sampled in order to calculate the conduction time of each leg according to (3). The PWM switching frequency generated by the digital controller and the sampling frequency of the input phase voltages are set to $f_s = 30$ kHz. First, we consider a representative case of a DC motor load. The parameters of the load are chosen to be $L_o = 1.5$ mH, $R_o = 20.3\ \Omega$ and $V_o = 12.4$ V. Several tests were carried out along with demonstration of the corresponding analytical results. Employing the solutions of $i_o[n, k]$ (25) and $i_o(\beta_n)$ (44) (see Appendix for details) simultaneously, the AC component of the output current, i_o, can be predicted, as shown in Fig. 10, for the following parameters: $V_{LL} = 100$ V and $M = 0.65$. In such an approach, $i_o[n, k]$ and $i_o(\beta_n)$ reflect the lower and upper envelope bounds of the actual response, respectively. As expected, one can see the presence of a sixth harmonic in i_o as a result of the bridge operation. Fig. 11 shows the experimental output current, i_o, AC component (sensed by the AC current probe) and the AC side input source waveforms, the input phase voltage v_T and the corresponding phase current, i_T. Fig. 11 confirms that the analytical approach predicted very well the behaviour of the experimental AC component, except for some negligible differences. Particularly, the measured

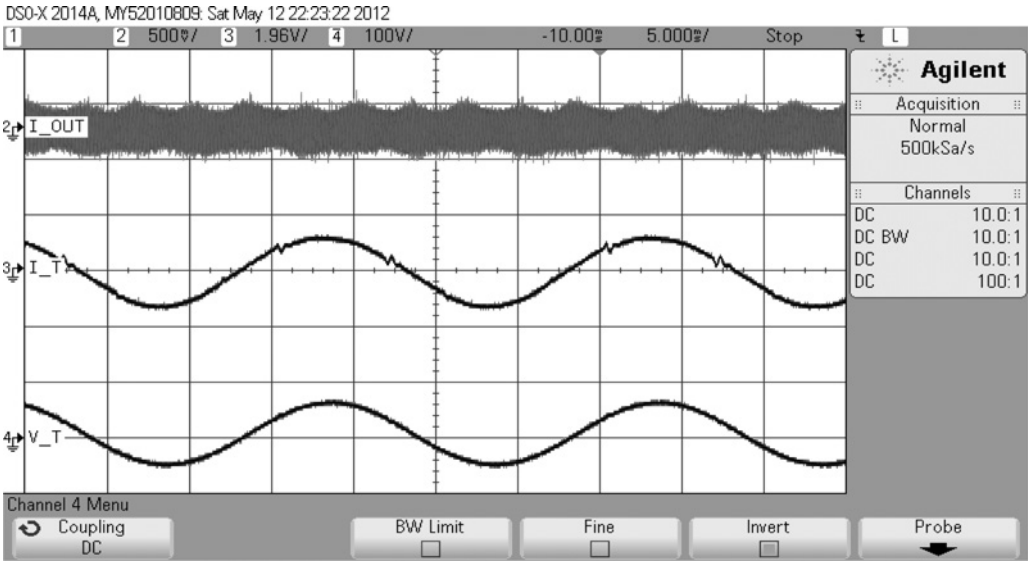

Fig. 11 *Typical experimental waveforms: output current i_o AC component (upper trace), input phase current i_T (middle trace) and input phase voltage v_T (lower trace)*

Vertical scale (upper trace): 0.5 A/div., vertical scale (middle trace): 1.96 A/div. and vertical scale (lower trace): 100 V/div., horizontal scale: 5 ms/div., with the same parameters as used in Fig. 10

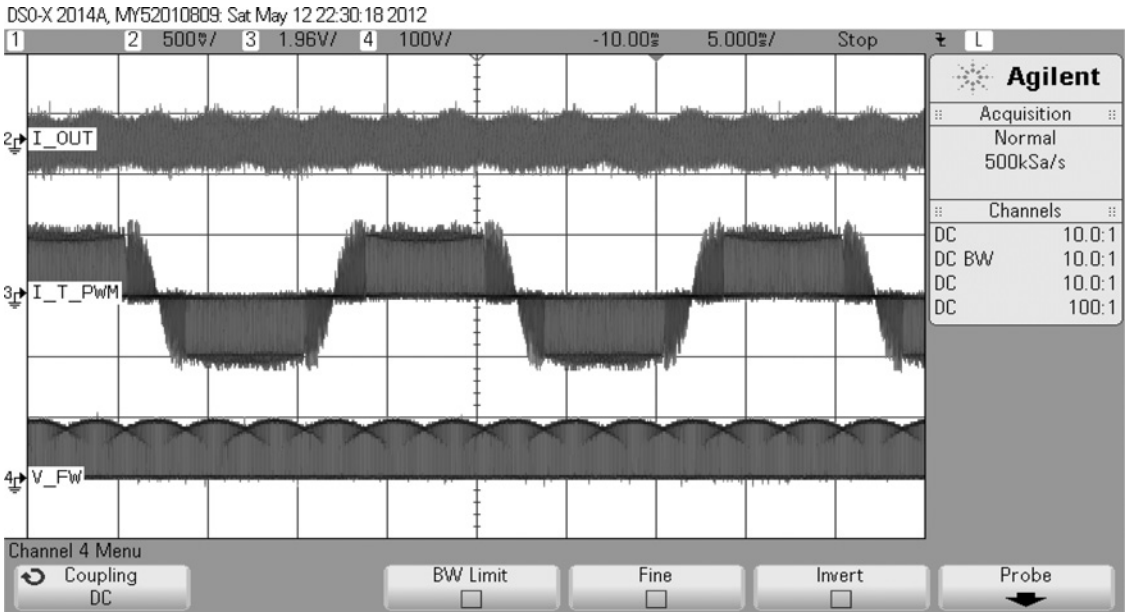

Fig. 12 *Typical experimental waveforms: output current i_o AC component (upper trace), the current through the switch Q_T (middle trace), freewheeling diode voltage v_{FW} (lower trace)*

Vertical scale (upper trace): 0.5 A/div., vertical scale (middle trace): 1.96 A/div., vertical scale (lower trace): 100 V/div., horizontal scale: 5 ms/div. with the same parameters as used in Fig. 10

doi: 10.1049/iet-pel.2011.0361

ripple seen in Fig. 11 is ~0.5 A, whereas the analytical result shown in Fig. 10 corresponds very well with the same value. It is also evident from Fig. 11 that the phase voltage, v_T, and the respective input current, i_T, are in phase as a result of the application of the modulation low (3), as discussed in Section 2, and hence guarantee a nearly unit power factor. In addition, Fig. 11 implies adequate quality of the input current, i_T. The experimental total harmonic distortion (THD) and the power factor were measured to be 0.8% and 0.990, respectively. Fig. 12 shows typical experimentally obtained time behaviour of the pulsating current through the switch, Q_T, and the freewheeling diode voltage, v_{FW}, recorded for the setup conditions described above.

A second set of experiments was carried out with $L_o = 12$ mH, $R_o = 8\ \Omega$ to represent the parameters of a stove. Without loss of generality, the constant voltage component has been set to $V_o = 0$ V. Clearly, this has no effect on the dynamics of the rectifier. Figs. 13 and 14 depict the experimentally obtained transient response of the output current for a step δ_m in modulation index from $M = 0.5$ to 0.6 and from $M = 0.5$ to 0.7, respectively. According to Figs. 13 and 14, the measured settling time is about 7 ms. In comparison, Figs. 15 and 16 reveal that the settling time of the respective analytical results using (25) and (44) are approximately the same at 7 ms. Here, we also observe good correspondence between the theoretical solution and the experimental data. The small discrepancy between the shape proportions of the measured and the predicted waveforms could be the result of modulation errors, input phase voltages distortion or series inductance differences, as well as because of the fact that the forward voltages of the semiconductor devices in the analytical approach and in the experiment were not the same. The experimental THD and power factor were measured to be

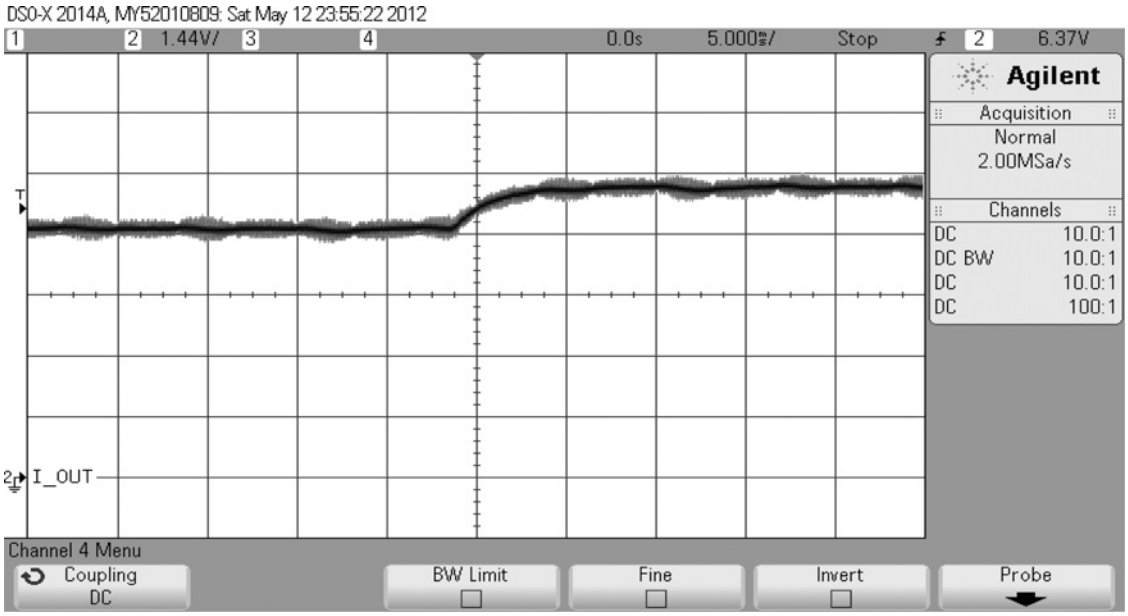

Fig. 13 *Experimental waveform of the output current i_o for a step $\delta_m = 0.1$ in modulation index, $M = 0.5$ to $M = 0.6$ with the following parameter values: $L_o = 12$ mH, $R_o = 8\ \Omega$, $V_o = 0$ V, $f_L = 50$ Hz, $f_s = 30$ kHz, and $V_{LL} = 100$ V*

Vertical scale: 1.44 A/div., horizontal scale: 5 ms/div

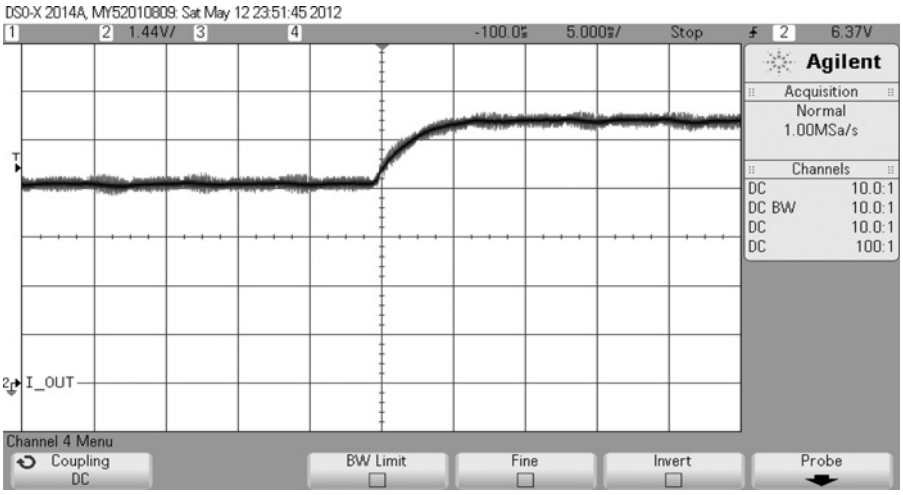

Fig. 14 *Experimental waveform of the output current i_o for a step $\delta_m = 0.2$ in modulation index, $M = 0.5$ to $M = 0.7$ with the following parameter values: $L_o = 12$ mH, $R_o = 8\ \Omega$, $V_o = 0$ V, $f_L = 50$ Hz, $f_s = 30$ kHz, and $V_{LL} = 100$ V*

Vertical scale, 1.44 A/div., horizontal scale, 5 ms/div

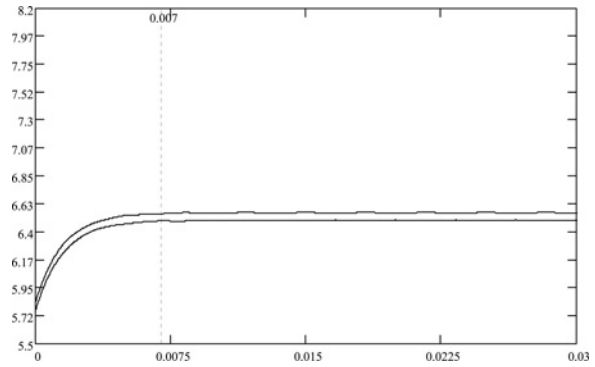

Fig. 15 *MathCAD's waveform of the output current i_o for a step $\delta_m = 0.1$ in modulation index, $M = 0.5–0.6$ with the same parameters as used in Fig. 13*

Units: amperes against seconds

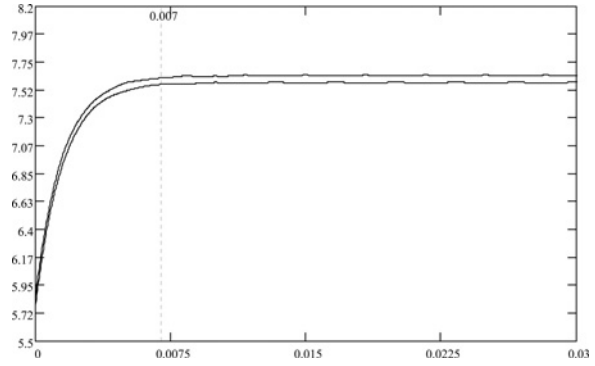

Fig. 16 *MathCAD's waveform of the output current i_o for a step $\delta_m = 0.2$ in modulation index, $M = 0.5–0.7$ with the same parameters as used in Fig. 14*

Units: amperes against seconds

1.8% and 0.998, respectively, for the same setup but with $M = 0.5$.

7 Conclusions

An accurate analysis of a three-phase buck rectifier with a resistor, inductor and constant voltage loading is carried out in this paper. A high frequency PWM template was used for the operation of the rectifier. It has been shown that using the difference equation method it is possible to obtain a closed form solution of the output current in both transient and steady-state operation modes. The theoretical solution of the load current provides the essential information on design quantities with which a three-phase buck rectifier circuit can be effectively designed. Mathcad calculated results, PSIM simulated measurements and experimental waveforms were used to validate the accuracy of the theoretical results.

For the sake of brevity and simplicity, the present paper was confined to a PWM rectifier with zero forward voltage drops across the semiconductor devices. With little effort, the proposed approach can be expanded to take these forward drops into account. In practice, the voltage drops cause to a voltage reduction across the DC-side freewheeling diode, as seen in (14)–(16), leading to efficiency degradation and distorted output currents. The major effect of this non-ideality on the accuracy of the analytical approach can be regarded as a constant DC voltage error on the DC side circuitry. Readers are referred to [2] for in-depth efficiency analysis of the rectifier. For simplicity, the analysis was carried out under the assumption that $L_F = C_F = 0$. The assumption was introduced mainly in order to simplify the mathematics involved in the analysis carried throughout this study. This assumption is valid for micro-scale wind turbine generators [10] and for true three-phase AC sources. To the best of the authors' knowledge, the subject presented herein has received limited attention over the years. Therefore in order to emphasise the essence of the method, it was necessary to reduce the complexity of the system thus eliminating the need to address higher order effects such as series inductances at the source input. In future studies, we will vary these parameters in order to refine the analysis. Likewise, the accuracy of the small signal analytical model can be improved by the inclusion of the input filter and other parasitical effects. Nevertheless, we found that the theoretical results obtained are quite accurate despite the simplifications that were made.

8 Acknowledgments

This research was supported by The Israel Science Foundation (grant no. 476/08) and by the Paul Ivanier Center for Robotics and Production management.

9 References

1 Koutroulis, E., Kalaitzakis, K.: 'Design of a maximum power tracking system for wind-energy-conversion applications', *IEEE Trans. Ind. Electron.*, 2006, **53**, (2), pp. 486–494
2 Nussbaumer, T., Baumann, M., Kolar, J.W.: 'Comprehensive design of a three-phase three-switch buck-type PWM rectifier', *IEEE Trans. Power Electron.*, 2007, **22**, (2), pp. 551–562
3 Krihely, N., Ben-Yaakov, S.: 'Modeling and evaluation of diode reverse recovery in discrete-transition simulators'. Proc. IEEE Energy Conversion and Exposition (ECCE), Atlanta, Georgia, USA, 12–16 September 2010, pp. 4514–4520
4 Caliskan, V., Perreault, D.J., Jahns, T.M., Kassakian, J.G.: 'Analysis of three-phase rectifiers with constant-voltage loads', *IEEE Trans. Circuits Syst.* I, *Fundam. Theory Appl.*, 2003, **50**, (9), pp. 1220–1226
5 Pejovic, P., Kolar, J.W.: 'Exact analysis of three-phase rectifiers with constant voltage loads', *IEEE Trans. Circuits Syst.* II, *Express Briefs*, 2008, **55**, (8), pp. 743–747
6 Klima, J., Skramlik, J., Valouch, V.: 'An analytical modeling of three-phase four-switch PWM rectifier under unbalanced supply conditions', *IEEE Trans. Circuits Syst.* II, *Express Briefs*, 2007, **54**, (12), pp. 1155–1159
7 Tooth, D.J., Finney, S.J., Williams, B.W.: 'Effects of using DC-side average current-mode control on a three-phase converter with an input filter and distorted supply'. Proc. Electric Power Application, 2000, pp. 459–468
8 Shoihet, A., Slonim, M.A.: 'Analysis of buck converter processes using difference equations methods'. IEEE 26th Convention of Electrical and Electronics Engineers in Israel (IEEEI), 2010, pp. 119–123
9 Slonim, M.A., Van-Wyk, J.D., Schoeman, J.J.: 'Analysis of transient and steady-state processes in the series resonant inverter', *Int. J. Electron.*, 1988, **64**, (2), pp. 323–332
10 Pan, C.T., Juan, Y.L.: 'A novel sensorless MPPT controller for a high-efficiency microscale wind power generation system', *IEEE Trans. Energy Convers.*, 2010, **25**, (1), pp. 207–216
11 Ilic, M., Maksimovic, D.: 'Interleaved zero-current-transition buck converter', *IEEE Trans. Ind. Appl.*, 2007, **43**, pp. 1619–1627
12 PSIM user manual, Powersim Inc., Version 8.0, 2009

10 Appendix

10.1 Derivation of the equivalent difference (25)

The expression of the equivalent difference (25) can be obtained by connecting the boundaries of the three

topologies (Fig. 4) over $k\pi/3 + n\Delta \le \theta \le k\pi/3 + (n+1)\Delta$ for any value of k and n as follows.

Substituting $\theta = k\pi/3 + n\Delta + \alpha_n$ into (19) we obtain

$$i_o(\alpha_n) = i_o[n, k]\, e^{-\alpha_n/\omega_L\tau} + \frac{V_{LL}\cos(n\Delta - (\pi/6)) - V_o}{R_o}[1 - e^{-\alpha_n/\omega_L\tau}] \quad (41)$$

where $i_o(\alpha_n) = i_o(\theta = k\pi/3 + n\Delta + \alpha_n)$.

Substituting $\theta = k\pi/3 + n\Delta + \alpha_n + \beta_n$ into (22), we obtain

$$i_o(\beta_n) = i_o(\alpha_n)\, e^{-\beta_n/\omega_L\tau} + \frac{V_{LL}\cos[n\Delta - (\pi/6) + (\pi/3)(-1)^{\varepsilon}] - V_o}{R_o} \times [1 - e^{-\beta_n/\omega_L\tau}] \quad (42)$$

where $i_o(\beta_n) = i_o(\theta = k\pi/3 + n\Delta + \alpha_n + \beta_n)$.

Substituting $\theta = k\pi/3 + (n+1)\Delta$ into (24), we obtain

$$i_o[n+1, k] = i_o(\beta_n)\, e^{-(\Delta - \alpha_n - \beta_n)/\omega_L\tau} - \frac{V_o}{R_o}\left[1 - e^{-(\Delta - \alpha_n - \beta_n)/\omega_L\tau}\right] \quad (43)$$

Substituting (41) into (42), we obtain (see (44))

Rearranging, we obtain

$$i_o(\beta_n) = i_o[n, k]\, e^{-(\alpha_n + \beta_n)/\omega_L\tau} + \frac{V_{LL}\cos(n\Delta - (\pi/6)) - V_o}{R_o} e^{-\beta_n/\omega_L\tau} - \frac{V_{LL}\cos(n\Delta - (\pi/6)) - V_o}{R_o} e^{-(\alpha_n + \beta_n)/\omega_L\tau} + \frac{V_{LL}\cos[n\Delta - (\pi/6) + (\pi/3)(-1)^{\varepsilon}] - V_o}{R_o} \times [1 - e^{-\beta_n/\omega_L\tau}] \quad (45)$$

By combining (45) and (43) the expression of $i_o[n+1, k]$ will have the following form

$$\begin{aligned} i_o[n+1, k] = {} & i_o[n, k]\, e^{-\Delta/\omega_L\tau} \\ & + \frac{V_{LL}\cos(n\Delta - (\pi/6)) - V_o}{R_o} e^{-(\Delta - \alpha_n)/\omega_L\tau} \\ & - \frac{V_{LL}\cos(n\Delta - (\pi/6)) - V_o}{R_o} e^{-\Delta/\omega_L\tau} \\ & + \frac{V_{LL}\cos[n\Delta - (\pi/6) + (\pi/3)(-1)^{\varepsilon}] - V_o}{R_o} \\ & \times e^{-(\Delta - \alpha_n - \beta_n)/\omega_L\tau} \\ & - \frac{V_{LL}\cos[n\Delta - (\pi/6) + (\pi/3)(-1)^{\varepsilon}] - V_o}{R_o} \\ & \times e^{-(\Delta - \alpha_n)/\omega_L\tau} - \frac{V_o}{R_o}\left[1 - e^{-(\Delta - \alpha_n - \beta_n)/\omega_L\tau}\right] \end{aligned} \quad (46)$$

It is evident that (46) is equivalent to (25).

$$i_o(\beta_n) = \left\{ i_o[n, k] e^{-\alpha_n/\omega_L\tau} + \frac{V_{LL}\cos(n\Delta - (\pi/6)) - V_o}{R_o}[1 - e^{-\alpha_n/\omega_L\tau}] \right\} e^{-\beta_n/\omega_L\tau} + \frac{V_{LL}\cos[n\Delta - (\pi/6) + (\pi/3)(-1)^{\varepsilon}] - V_o}{R_o}[1 - e^{-\beta_n/\omega_L\tau}] \quad (44)$$